Prometheus and Pandora:
masses and orbital positions during the *Cassini* tour

Stéfan Renner [a,*], Bruno Sicardy [a], Richard G. French [b]

[a] *LESIA, Observatoire de Paris, Bâtiment 10, 5, place Jules Janssen, FR-92195 Meudon cedex, France*
[b] *Astronomy Department, Wellesley College, Wellesley, MA 02481, USA*

Abstract

Hubble Space Telescope (*HST*) images of Prometheus and Pandora show longitude discrepancies of about $20°$ with respect to the *Voyager* ephemerides, with an abrupt change in mean motion at the end of 2000 (French et al., 2003, Icarus 162, 143–170; French and McGhee, 2003, Bull. Am. Astron. Soc. 34, 06.07). These discrepancies are anti-correlated and arise from chaotic interactions between the two moons, occurring at interval of 6.2 yr, when their apses are anti-aligned (Goldreich and Rappaport, 2003a, Icarus 162, 391–399). This behavior is attributed to the overlap of four 121:118 apse-type mean motion resonances (Goldreich and Rappaport, 2003b, Icarus 166, 320–327). We study the Prometheus–Pandora system using a Radau-type integrator taking into account Saturn's oblateness up to and including terms in J_6, plus the effects of the major satellites. We first confirm the chaotic behavior of Prometheus and Pandora. By fitting the numerical integrations to the *HST* data (French et al., 2003, Icarus 162, 143–170; French and McGhee, 2003, Bull. Am. Astron. Soc. 34, 06.07), we derive the satellite masses. The resulting *GM* values (with their standard 3-σ errors) for Prometheus and Pandora are respectively $GM_{\mathrm{PR}} = (1.41^{+0.10}_{-0.25}) \times 10^{-2}$ and $GM_{\mathrm{PA}} = (1.03^{+0.10}_{-0.19}) \times 10^{-2}$ km³ s⁻². Using the nominal shape of the two moons (Thomas, 1989, Icarus 77, 248–274), we derive Prometheus and Pandora's densities, $0.40^{+0.03}_{-0.07}$ and $0.49^{+0.05}_{-0.09}$ g cm⁻³, respectively. Our numerical fits also enable us to constrain the time of the latest apse anti-alignment in 2000. Finally, using our fit, we predict the orbital positions of the two satellites during the *Cassini* tour, and provide a lower limit of the uncertainties due to chaos. These uncertainties amount to about $0.2°$ in mean longitude at the arrival of the *Cassini* spacecraft in July 2004, and to about $3°$ in 2008, at the end of the nominal tour.

© 2004 Elsevier Inc. All rights reserved.

Keywords: Satellites of Saturn; Celestial mechanics; Orbits; Chaos; Resonances

1. Introduction

Saturn's narrow F ring is flanked by two small moons, Prometheus and Pandora, discovered in *Voyager* images taken in 1980 and 1981. They were originally hailed as examples of shepherd satellites, according to the theory developed to account for the confinement of Uranus' rings (Goldreich and Tremaine, 1979). However, the details of the mechanism by which Prometheus and Pandora could confine the ring are poorly understood, because the dynam-

ics of the F ring is much more complex (overlapping resonances, interactions or collisions with Prometheus, etc.) than its uranian counterparts. Nevertheless, the dynamical behavior of Prometheus and Pandora and their interactions with the F ring have been extensively investigated theoretically (Dermott, 1981; Showalter and Burns, 1982; Lissauer and Peale, 1986; Kolvoord et al., 1990; Murray and Giuliatti Winter, 1996; Murray et al., 1997; Namouni, 1998; Showalter et al., 1999a, 1999b; Giuliatti Winter et al., 2000; Poulet and Sicardy, 2001; Showalter, 2004).

Orbits for Prometheus and Pandora were fitted to *Voyager* data (Synnott et al., 1981, 1983) in the form of precessing ellipses. Mean motions were determined from images and precession rates were calculated to be consistent with the

---

* Corresponding author. Fax: +33-1-4507-7110.
E-mail address: stefan.renner@obspm.fr (S. Renner).

gravity field of the saturnian system (Nicholson and Porco, 1988; Campbell and Anderson, 1989).

Observations with the Hubble Space Telescope (*HST*) made during the 1995–1996 Sun and Earth ring plane crossings led to the discovery that Prometheus was lagging its predicted longitude based on the *Voyager* ephemeris by about 20° (Bosh and Rivkin, 1996; Nicholson et al., 1996). Subsequently, Pandora was found to lead the *Voyager* ephemeris prediction by a similar amount (McGhee, 2000). These discrepancies were confirmed by several authors (Murray et al., 2000; McGhee et al., 2001; French et al., 2003). In particular, French et al. (2003) derived sky-plane positions using archival *HST* data from 1994, together with unexamined ring plane crossing images, and a large series of targeted WFPC2 observations between 1996 and 2002. These positions were then compared to the predictions of revised and improved ephemerides for the two satellites based on an analysis of the full set of *Voyager* images (Evans, 2001). From December 1994 to December 2000, Prometheus and Pandora orbital longitude offsets were changing at rates of $-0.71°$ and $+0.44°$ yr^{-1}, respectively, relative to the new *Voyager* ephemerides. An additional oscillatory component due to the nearby 3:2 co-rotation resonance with Mimas was evident in the longitude of Pandora. Orbital elements for freely precessing equatorial orbits were determined from fits to the 1994–2000 observations. Moreover, a new twist in the meanderings of the two moons occurred around the end of 2000: the mean motions of Prometheus and Pandora changed suddenly by an additional -0.77 and $+0.92°$ yr^{-1}, respectively (French et al., 2003).

The longitude discrepancies have comparable magnitude and opposite signs, suggesting direct gravitational interactions between the two satellites. Goldreich and Rappaport (2003a) confirmed that expectation and showed that the orbits were chaotic. Numerical integrations including Prometheus, Pandora and Saturn's gravitational oblateness yield a Lyapunov exponent of order 0.3 yr^{-1}, for satellite masses based on a nominal density of 0.63 g cm^{-3}, the value of Epimetheus' density (Nicholson et al., 1992). Chaotic interactions occur when the orbits come closest together, which happens at intervals of 6.2 yr when their apses are anti-aligned. At these times, sudden changes in mean motions appear in numerical integrations, showing that the changes in the mean motions of Prometheus and Pandora observed at the end of 2000 occurred around the time their apsidal lines were anti-aligned. The chaotic orbits of Prometheus and Pandora were subsequently shown to be due to the overlap of four apse-type 121:118 mean motion resonances (Goldreich and Rappaport, 2003b). A model with 1.5 degrees of freedom was used to show that the Lyapunov exponent of 0.3 yr^{-1} arises because the critical argument of the dominant member of the resonant quartet makes approximately two separatrix crossings every 6.2 yr precessional cycle.

Numerical integrations including the effects of the eight major satellites of Saturn confirmed the chaotic orbits and the anti-correlation in the temporal variation of the mean longitudes of Prometheus and Pandora (Renner and Sicardy, 2003; Cooper and Murray, 2004). The effects of the nearby Mimas 3:2 resonances were clearly detectable. Cooper and Murray (2004) also showed that there was an evidence in the simulations that the co-orbitals Janus and Epimetheus have a role in the dynamical evolution of Prometheus and Pandora, via two independent sets of second-order resonances (17:15 and 21:19) due to Epimetheus, which contribute to the chaotic motions on a longer timescale. French et al. (2003) reached a similar conclusion about the possible role of the 17:15 and 21:19 resonances with the co-orbitals. Comparison of the results of Cooper and Murray (2004) with extrapolations of current published ephemerides suggested uncertainties on the order of 4° in the mean longitudes of Prometheus and Pandora during the *Cassini* tour.

In the present work, we first confirm the chaotic motions of Prometheus and Pandora (Section 3) using a numerical model that takes into account the effects of Saturn's oblateness (up to J_6) and the perturbations by the major satellites, including the co-orbital moons Janus and Epimetheus. This numerical model and the full initial conditions used are presented in Section 2. Then, by fitting the numerical integrations to the *HST* data, we derive the satellite masses (Section 4). Finally, in Section 5, we use our fit to provide the orbital positions of Prometheus and Pandora, together with the uncertainties due to chaos, during the *Cassini* tour.

2. Numerical model

2.1. Overview

To study the dynamical behavior of Prometheus and Pandora, we use the *Mercury* 6 integrator package (Chambers, 1999), with Everhart's *Radau* algorithm (Everhart, 1985), and an accuracy parameter $\delta = 10^{-12}$, the error per step the algorithm tolerates. Our model includes the following satellites (in increasing order of distance from the planet): Prometheus, Pandora, Epimetheus, Janus, Mimas, Enceladus, Tethys, Dione, Rhea, Titan, and Iapetus. The effects of the planet's oblateness are taken into account up to and including terms in J_6. The full equations of motion are integrated in a Saturn-centered cartesian reference frame ($O\mathbf{XYZ}$), where ($O\mathbf{XY}$) is the equatorial plane of Saturn, $\mathbf{X}$ the ascending node of Saturn's equator on the mean Earth equator at $J2000$ (epoch JED 2451545.0 = 2000 January 1.5), $\mathbf{Z}$ the Saturn's pole direction at $J2000$, defined by the equatorial coordinates $\alpha_P = 40.5955°$ and $\delta_P = 83.53812°$ (French et al., 1993), and $\mathbf{Y} = \mathbf{Z} \times \mathbf{X}$.

2.2. Initial conditions

All integrations start at epoch JED 2449940.0 = 1995 August 10.5 (at Saturn), because the orbital elements of

Prometheus, Pandora, and the co-orbitals Janus and Epimetheus are given at this epoch (see below). We use the physical parameters of Saturn (mass, radius and oblateness up to and including J_6) given in Table 1, derived by Campbell and Anderson (1989) from the analysis of *Pioneer* and *Voyager* data.

The orbital elements of Prometheus and Pandora are derived by French et al. (2003), at epoch JED 2449940.0, and are reproduced in Table 2. These elements hold for freely precessing equatorial orbits from fits to *HST* observations for the period December 1, 1994 through December 6, 2000. In our simulations, the eccentricity and the mean longitude of Prometheus and Pandora are fixed at the nominal values given by French et al. (2003). As explained in Section 4, a wide range of initial values are used for the other elements (semi-major axis and longitude of periapsis, assuming equatorial orbits) to fit the satellite masses to the *HST* observations. In the case of Janus and Epimetheus, we use the orbital elements given in Table 2, derived by McGhee et al. (2001) at epoch JED 2449940.0. They also result from fits to *HST* observations for freely precessing equatorial orbits, during the 1995 ring plane crossings.

The longitudes of Prometheus, Pandora, Epimetheus and Janus are measured in the equatorial plane ($O\mathbf{XY}$) of Saturn, from the ascending node of Saturn's equator at epoch on the mean Earth equator at $J2000$; that is, from the unit $\mathbf{X}$ vector defined above. Before each numerical simulation, we perform transformations that convert the *geometric* orbital elements of these satellites into state vectors in the

($O\mathbf{XYZ}$) Saturn-centered reference frame. These transformations, not detailed here, arise from the epicyclic theory (Borderies and Longaretti, 1987; Longaretti and Borderies, 1991; Borderies-Rappaport and Longaretti, 1994) and are accurate to second order in eccentricity. They are also used to compute, conversely, the geometric orbital elements of the satellites from the state vectors given by the numerical integrations. Such computations require the iterative calculation of some basic frequencies such as the mean motion n, the apsidal precession rate of the satellite $\dot{\varpi}$ and, if we consider non-equatorial orbits, the precession rate of the ascending node $\dot{\Omega}$. Expressions for n and $\dot{\varpi}$ are reproduced in Appendix A.

For the other satellites, we use the semi-analytic theory *TASS*1.6 (Vienne and Duriez, 1995) to derive the initial conditions at epoch JED 2449940.0. With *TASS* the output data is the position and the velocity of the body in a Saturn-centered cartesian reference frame ($O\mathbf{X'Y'Z'}$), where $\mathbf{X'}$ is the $J2000$ mean equinox and $\mathbf{Z'}$ the $J2000$ ecliptic pole. Therefore, to set all the satellites in the same reference frame ($O\mathbf{XYZ}$) described in the previous section, we apply the following three rotations:

$$\begin{bmatrix} X \\ Y \\ Z \end{bmatrix} = R_\Omega(\pi/2 - \delta_P) \times R_{P_T}(\pi/2 + \alpha_P)$$

$$\times R_\gamma(-\epsilon) \begin{bmatrix} X' \\ Y' \\ Z' \end{bmatrix}, \tag{1}$$

where $R_V(\beta)$ denotes a rotation through a positive angle β about the V axis, ϵ is the Earth obliquity at $J2000$ ($\epsilon = 23°26'21.411''$, *IERS* value), α_P and δ_P are the equatorial coordinates of Saturn's $J2000$ pole direction (French et al., 1993), γ is the mean equinox at $J2000$, P_T is the Earth's pole at $J2000$, and Ω is the ascending node of Saturn's equator at epoch on the mean Earth equator at $J2000$.

Table 1
Physical parameters of Saturn, from Campbell and Anderson (1989)

R_S (km)	60330
GM_S (km^3 s^{-2})	37931272
J_2	16298×10^{-6}
J_4	-915×10^{-6}
J_6	103×10^{-6}

Table 2
Orbital elements for the inner satellites, at epoch JED 2449940.0

	Prometheus	Pandora	Janus	Epimetheus
Epoch (JED)	2449940.0	2449940.0	2449940.0	2449940.0
a (km)	139377.624	141713.1075	151461.99	151414.61
n (° day^{-1})	587.28747	572.78560	518.2383	518.4822
e	$(1.92 \pm 0.21) \times 10^{-3}$	$(4.5 \pm 0.3) \times 10^{-3}$	0.0066	0.0126
i (°)	0.0	0.0	0.0	0.0
Ω (°)	–	–	–	–
ϖ (°)	257 ± 10	359 ± 6	107.95	222.95
λ (°)	339.155	96.023	35.33	175.33

Prometheus and Pandora orbital elements result from fits to *HST* observations for the period December 1, 1994 through December 6, 2000 (French et al., 2003). Quoted errors (in periapsis and eccentricity) are three times the formal σ of the fit. The longitudes are measured from the ascending node of Saturn's equator at epoch on the mean Earth equator at $J2000$. Saturn's equatorial plane at epoch is defined relative to Saturn's $J2000$ pole direction $\alpha_P = 40.5955°$, $\delta_P = 83.53812°$ (French et al., 1993). The semi-major axis and mean motion are calculated self-consistently, using GM_S, J_2, and J_4 as given by Nicholson and Porco (1988). Orbits were assumed to be equatorial in the fits. Janus and Epimetheus orbital elements result from fits to *HST* observations, during the 1995 ring plane crossings, for freely precessing equatorial orbits (McGhee et al., 2001). The longitudes are also measured from the ascending node of Saturn's equator at epoch on the mean Earth equator at $J2000$, and the semi-major axis and mean motion are calculated self-consistently, using GM_S, J_2, and J_4 as given by Nicholson and Porco (1988). The eccentricity and the longitude of periapsis at epoch are computed using analytical ephemerides (Nicholson et al., 1992; Yoder et al., 1989).

Table 3
Satellite *GM* values

Satellite	GM (km^3 s^{-2})
Epimetheus	0.0357
Janus	0.1284
Mimas	2.4048
Enceladus	4.0586
Tethys	40.2071
Dione	74.4591
Rhea	163.8631
Titan	8927.5042
Iapetus	117.587

Values for the co-orbitals Janus and Epimetheus are from McGhee et al. (2001). For the other satellites they are derived from the results of *TASS*1.6 (Vienne and Duriez, 1995, Table 10), using the GM_S value of Saturn from Campbell and Anderson (1989). Because the mass of Enceladus is not well determined with *TASS*1.6, we arbitrarily adopt the value from *TASS*1.5, which is closer to previous determinations (Harper and Taylor, 1993; Dourneau, 1987).

Finally, the adopted values for the masses of the satellites are summarized in Table 3.

3. Confirmation of chaos

The chaotic behavior of Prometheus and Pandora, due to the overlap of four 121:118 apse-type mean motion resonances, has been demonstrated in a model consisting of the two satellites orbiting Saturn, including the effects of the planet's oblateness (Goldreich and Rappaport, 2003a, 2003b). The interactions of Prometheus and Pandora with the other satellites of Saturn were neglected. However, Prometheus and Pandora are involved in resonances with Mimas and with the co-orbitals Janus and Epimetheus: Pandora is close to a 3:2 co-rotation resonance and a 3:2 Lindblad resonance with Mimas, and Prometheus and Pandora are periodically perturbed (about every four years) by the second-order resonances 17:15 and 21:19 with Epimetheus, respectively. Here we show, in parallel to a recent numerical study (Cooper and Murray, 2004), that the chaotic interactions between the two moons survive the addition of the major satellites of Saturn to the model.

We present a typical result of numerical integrations in Figs. 1 and 2. The integration time is 20 yr, starting at epoch JED 2449940.0. The numerical model is described in Section 2, with all the initial conditions given in Section 2.2. In particular, Prometheus and Pandora are initially on equatorial orbits with nominal eccentricities and mean longitudes given in Table 2. For this simulation, the remaining initial conditions for Prometheus and Pandora are given in Table 4. These values actually correspond to our best-fit solution (see Section 4.2).

In Fig. 1, we give Prometheus and Pandora's mean longitude offsets (in degrees) from the predictions provided by the *Voyager* ephemerides, versus time (in days), as in French et al. (2003). Sudden and anti-correlated changes in mean motion are clearly apparent around the times of apse anti-
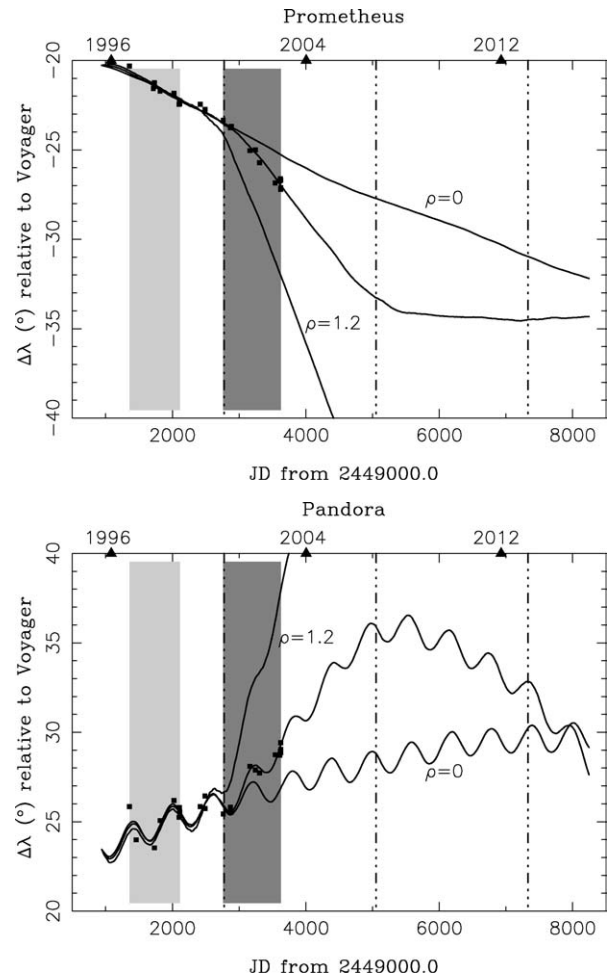
Fig. 1. Longitude offsets ($^\circ$) from *Voyager* predictions for Prometheus (top) and Pandora (bottom) versus time (days). The vertical dashed–dotted lines denote the times of apse anti-alignment, computed using the apsidal precession rates of the two satellites given in French et al. (2003). The years 1996, 2004, and 2012 are labeled on the top horizontal axis. The integration start time is 1995 August 10.5 (epoch JED 2449940.0). The middle solid curves correspond to the best-fit solution (Table 4). Two additional solutions are indicated, corresponding to satellite densities $\rho = 0$ and 1.2 g cm^{-3}. The $\Delta\lambda$'s are the difference between the mean longitude λ provided by the simulation and the mean longitude λ_{VGR} predicted by the ephemeris based on *Voyager* images (Evans, 2001). For Prometheus, $\lambda_{VGR}(^\circ) = \lambda_{VGR}^0 + n_{VGR}(t - t_0) = 188.526 + 587.28942(t - 2444839.6682)$ and for Pandora, $\lambda_{VGR} = 82.13 + 572.78439(t - 2444839.6682)$ (French et al., 2003; Evans, 2001). Each square point represents a separate set of *HST* data for which a single longitude offset $\Delta\lambda$ was computed, from the observed sky-plane coordinates. These points are affected by the satellite eccentricities, because for them we compute a true longitude, not a mean longitude, to derive $\Delta\lambda$ (Section 4.2). The light and dark grey areas denote two separate subsets of data for which we perform fits: with the first one we fit Prometheus and Pandora's semi-major axes, and with the second one the satellite masses and the longitudes of periapsis.

alignment (indicated by the vertical dashed-dotted lines). We also indicate two additional solutions corresponding to satellite densities $\rho = 0$ and 1.2 g cm^{-3}, respectively, clearly showing the effects of masses on the longitudinal variations of the satellites. The $\Delta\lambda$'s are, both for Prometheus and Pandora, the difference between the mean longitude λ provided by
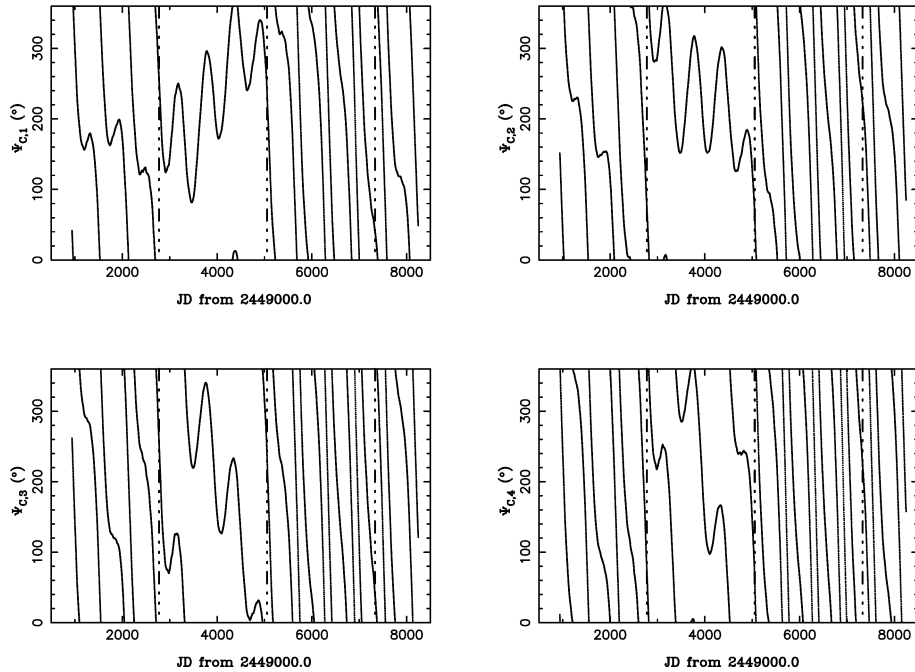
Fig. 2. 121:118 resonance arguments ($^\circ$) versus time (days), for the best-fit solution given in Fig. 1. The four critical angles are: $\Psi_{C,1} = 121\lambda_{PA} - 118\lambda_{PR} - 3\varpi_{PA}$, $\Psi_{C,2} = 121\lambda_{PA} - 118\lambda_{PR} - 2\varpi_{PA} - \varpi_{PR}$, $\Psi_{C,3} = 121\lambda_{PA} - 118\lambda_{PR} - \varpi_{PA} - 2\varpi_{PR}$, $\Psi_{C,4} = 121\lambda_{PA} - 118\lambda_{PR} - 3\varpi_{PR}$. The vertical dashed–dotted lines denote the times of apse anti-alignment. The integration start time is 1995 August 10.5.

by the simulation and the mean longitude λ_{VGR} predicted by the ephemeris based on *Voyager* images (Evans, 2001). Note that Pandora's *Voyager* ephemeris includes the effects of Mimas. Clearly apparent on the figure are also the wiggles in the mean longitude of Pandora, which are due to the nearby 3:2 co-rotation resonance with Mimas. Pandora's semi-major axis lies approximately 50 km inside this resonance, and also 180 km inside the 3:2 inner Lindblad resonance with Mimas. Some theoretical predictions on the effects of these two 3:2 resonances are given by French et al. (2003).

Note that Janus and Epimetheus have a dynamical influence on the orbits of Prometheus and Pandora (Cooper and Murray, 2004). These satellites move on horseshoe orbits. The consequence is a switch in their orbits every approximately 4 yr (Yoder et al., 1989; Nicholson et al., 1992). During their co-orbital motion, the radial deviations from their mean semi-major axis are ± 10 km for Janus and ± 40 km for Epimetheus. Prometheus and Pandora are involved in 17:15 and 21:19 second-order resonances with Epimetheus, respectively, especially when Epimetheus is in its inner position of the horseshoe orbit. When it is in its outer position, the 17:15 and 21:19 resonances move well outside the orbits of Prometheus and Pandora. Among the two triplets of critical arguments, the closest to libration are $17\lambda_{EP} - 15\lambda_{PR} - \varpi_{EP} - \varpi_{PR}$ for Prometheus, and $21\lambda_{EP} - 19\lambda_{PA} - 2\varpi_{PA}$ for Pandora, where the subscript EP denotes Epimetheus.

The four 121:118 resonant arguments between Prometheus and Pandora are displayed in Fig. 2. These critical angles are: $\Psi_{C,1} = 121\lambda_{PA} - 118\lambda_{PR} - 3\varpi_{PA}$, $\Psi_{C,2} = 121\lambda_{PA} - 118\lambda_{PR} - 2\varpi_{PA} - \varpi_{PR}$, $\Psi_{C,3} = 121\lambda_{PA} - 118\lambda_{PR} -$

$\varpi_{PA} - 2\varpi_{PR}$, and $\Psi_{C,4} = 121\lambda_{PA} - 118\lambda_{PR} - 3\varpi_{PR}$. The four resonances clearly overlap. Also evident are separatrix crossings around the times of the first two apse anti-alignments, where the critical angles go from a circulation motion to libration (or from libration to circulation motion). This confirms in a full integration the results of Goldreich and Rappaport (2003a) obtained in a simplified 2-satellite model.

4. Fits for satellite masses

4.1. Method

In order to derive Prometheus and Pandora's masses, we fit the numerical integrations to the *HST* data. More precisely, we want to find the initial orbital elements and the masses of Prometheus and Pandora, for which the residuals between the observations and the calculated satellite positions are minimal. This is a non-trivial problem of parameter estimation: the two satellites are a priori defined by seven parameters (six orbital elements plus the mass) and each initial orbital element has its own uncertainty. Moreover, Prometheus and Pandora are highly sensitive to initial conditions, because of chaos.

We use the *HST* data (French et al., 2003; French and McGhee, 2003) between 1995 August 10.5 (epoch JED 2449940.0) and 2002 December 17.5 (epoch JED 2452626.0). These data contain the sky-plane coordinates of Prometheus and Pandora (right ascension $\Delta\alpha\cos\delta$ and declination $\Delta\delta$ offsets from Saturn's center in *J*2000 co-

ordinates), together with the time (at Earth) of each image, the Earth–Saturn distance D, and 3 angles U, B, P which define the geometry of Saturn's rings and can be used to project the saturnicentric positions of the satellites into the plane of the sky. The angle U is the geocentric longitude of Saturn, measured in the plane of the rings eastward from its $J2000$ ascending node on the mean equator of the Earth (the saturnicentric longitude of the Earth, measured in the same way, is $U + 180°$). The angle B is the inclination of the ring plane, more precisely the saturnicentric latitude of the Earth referred to the plane of the rings, positive toward the north (when B is positive the visible surface of the rings is the northern surface). Finally, the angle P is the $J2000$ position angle of Saturn's pole, or the geocentric position angle of the northern semi-minor axis of the apparent ellipse of the rings, measured eastward from north.

To compare the simulations with the data, we compute a table of times at Saturn for which we have *HST* data, correcting for the light-time travel. Then at these times we store for Prometheus and Pandora the state vectors provided by the numerical integration in the Saturn-centered reference frame described in Section 2, with initial conditions given in Section 2.2. The position vectors are then used to compute our own sky-plane coordinates $\Delta\alpha\cos\delta$ and $\Delta\delta$. Let X, Y, Z be the components of the position vector of Prometheus or Pandora. Then the right ascension and declination offsets from Saturn's center, for equatorial orbits, are given by:

$$
\begin{cases}
\Delta\alpha\cos\delta = \big[-\cos P(X\sin U - Y\cos U) \\
\qquad + \sin B \sin P(X\cos U + Y\sin U)\big]/D, \\
\Delta\delta = \big[\sin P(X\sin U - Y\cos U) \\
\qquad + \sin B \cos P(X\cos U + Y\sin U)\big]/D.
\end{cases}
\tag{2}
$$

If we consider non-equatorial motions, then the terms $Z\cos B\sin P$ and $Z\cos B\cos P$ must be added to $\Delta\alpha\cos\delta$ and $\Delta\delta$, respectively, into the brackets. Finally, we compute the rms residual between the observed sky-plane coordinates and those provided by the simulation. Comparing the astrometric measurements to orbital predictions by R. Jacobson (personal communication), French and McGhee (2003) showed that the typical astrometric accuracy of the *HST* measurements is about $0.02''$, equivalent to errors in the positions of the satellites to about 130 km. Thus, for a "perfect" numerical model, we would expect an rms error of about $0.02''$.

We suppose that Prometheus and Pandora move on equatorial orbits. Based on the reanalysis of the full set of *Voyager* observations, Evans (2001) find inclinations for Prometheus and Pandora of $0.03° \pm 0.005°$ and $0.054° \pm 0.007°$, respectively. These inclinations correspond to maximum excursions from the equatorial plane of 73 and 134 km, comparable to the *HST* measurement accuracy. The small inclinations of the two satellites are thus neglected in this work, and also in French et al. (2003) because they are at the edge of detectability in the data. On the other hand, because the mean longitudes are well constrained by the observations, they are initially fixed at the nominal values given

in Table 2. Fits of the satellite eccentricities to subsets of *HST* data yield similar values to the solutions of French et al. (2003), and the residuals are not very sensitive to these eccentricity values (see Section 4.2). Moreover, the changes in eccentricity associated with the interactions of Prometheus and Pandora are very small in comparison to the mean eccentricities (Goldreich and Rappaport, 2003a). Therefore, the eccentricities are also fixed at the nominal values given in Table 2. Consequences of this assumption on our mass determinations are discussed in Section 4.2.

Thus, the adjustment of the numerical integrations to the *HST* data now depends only on the initial semi-major axes and periapse longitudes. In fact, the key parameters are only the initial semi-major axes and the initial difference in longitude of periapsis $\Delta\varpi_0 = \varpi_{PR} - \varpi_{PA}$ $[2\pi]$, the only parameter that provides the time of apse anti-alignment. The motion of Prometheus and Pandora during the period of the *HST* data can be split into two parts: a period of regular motion, far from any apse anti-alignment, for which the orbits are essentially precessing keplerian ellipses, and a period of chaotic motion, around the time of apse anti-alignment. Indeed, we do not detect in our simulations significant variations in longitude far from the times of apse anti-alignments (see Figs. 1 and 4). The regular part of the data is sensitive to the initial semi-major axes, and the chaotic part to the masses and to the initial difference in longitude of periapsis, $\Delta\varpi_0$. To derive the satellite masses, we therefore perform two consecutive fits on different subsets of data. First we determine the initial semi-major axes that minimize the rms residuals during the period of regular motion, and then we fit the masses and the initial difference in longitude of periapsis on the chaotic part of the *HST* data.

The fit of the simulations to the regular part of the *HST* data (that is, the adjustment of the initial semi-major axes) does not contain any information on the satellite masses. Indeed, given satellite masses, one can always find initial semi-major axes that fit this part of the data quite well. More precisely, the initial semi-major axis of one of the two satellites depends linearly (at least at lowest order, see Eqs. (3)) on the mass of the other satellite: suppose that Prometheus and Pandora move on a given orbit, and let us increase the mass of Prometheus. This creates an additional acceleration to Pandora that tends to decrease its radius, Prometheus being inside the orbit of Pandora. Therefore, the initial semi-major axis of Pandora must be slightly increased in order the orbit of Pandora to remain unchanged. In the same manner, because Pandora evolves outside the orbit of Prometheus, the initial semi-major axis of Prometheus must be decreased if the mass of Pandora is increased. After this first step, we can analytically derive the appropriate initial semi-major axes, given the satellite masses, to fit correctly the regular part of the *HST* data.

The regular and chaotic part of the data used to fit the remaining orbital elements (semi-major axes and periapsis longitudes) and the masses are indicated in Fig. 1 by the light and dark grey areas, respectively. The first period is

between 1996 September 30 (epoch JED 2450356.5) and 1998 October 24 (epoch JED 245110.5), which is far from any apse anti-alignment, the second is between 2000 August 4 (epoch JED 2451760.5) and 2002 December 17.5 (epoch JED 2452626.0), which contain the anti-correlated bends observed in the longitude profiles of Prometheus and Pandora. Note that with our simulations, it is useless to consider a much greater time interval to fit the satellite masses, because the integration start time is 1995 August 10.5 and the Lyapunov time of the system is only about three years. For information, the number of data points is 49 and 34 for Prometheus and Pandora, respectively, during the regular motion period, and 97 and 94, respectively, during the chaotic period.

4.2. Results

For each simulation we compute a rms error, which is the average of Prometheus and Pandora's rms residuals. By fitting the numerical integrations to the regular part of the *HST* data (light grey area of Fig. 1), we have derived empirically the following relations between the initial semi-major axes (km) and the satellite *GM* values (km³ s⁻²), for which the rms error is minimal:

$$\begin{cases} a_{\mathrm{PR}} = 139377.5 - 5.96 GM_{\mathrm{PA}} = 139377.5 - 0.125\rho_{\mathrm{PA}}, \\ a_{\mathrm{PA}} = 141714.18 + 7.11 GM_{\mathrm{PR}} = 141714.18 + 0.25\rho_{\mathrm{PR}}. \end{cases}$$
(3)

As noted in the previous section, these relations are linear. Using ellipsoidal models, Thomas (1989) derived the following satellite radii: 74, 50, and 34 km for Prometheus, and 55, 44, and 31 km for Pandora. We have used these nominal shapes to write the relations in Eqs. (3) using the densities ρ (g cm⁻³). The longitudes of periapsis were fixed at the nominal values of Table 2, yielding an initial difference in longitude of periapsis $\Delta\varpi_0 = 258°$. The relation for a_{PR} (respectively a_{PA}) was derived supposing $M_{\mathrm{PR}} = 0$ (respectively $M_{\mathrm{PA}} = 0$), and would be approximately the same for $M_{\mathrm{PR}} \neq 0$ (respectively $M_{\mathrm{PA}} \neq 0$). Typically, using these relations, the rms error is about 0.030″, with comparable individual residuals for Prometheus and Pandora.

The correction terms in Eqs. (3) are small: 150 and 300 m at most for Prometheus and Pandora, respectively, for a density $\rho = 1.2$ g cm⁻³. However, the rms residuals are very sensitive to the initial semi-major axes when fitting the regular part of the data. Let us suppose that $M_{\mathrm{PR}} = 0$. For a given mass of Pandora M_{PA}, the rms residual for Prometheus, as a function of its initial semi-major axis, is a parabolic-shaped curve, with a minimal value ($\simeq 0.03″$) for a semi-major axis $a_{\mathrm{PR}}^{\min}$ given by the linear relation in Eqs. (3). A difference of only about ±50–80 m from $a_{\mathrm{PR}}^{\min}$, depending on the value of Pandora's density, yields a rms error of about 0.08″, that is 4 times the astrometric accuracy of the *HST* measurements. This is because a small change in semi-major axis translates into large longitude offsets over the years.

Then we performed fits to the chaotic part of the data (dark grey area of Fig. 1), to derive the satellite masses

and the longitudes of periapsis. We have considered values of $\Delta\varpi_0$ in the range $242° \leqslant \Delta\varpi_0 \leqslant 274°$, to be consistent with the uncertainties of Prometheus and Pandora's periapse longitudes derived in French et al. (2003), see Table 2. We used a step of one degree, which corresponds to a difference of about 6.33 days between the times of two apse anti-alignments, using apsidal precession rates given by French et al. (2003). The interval of masses for these simulations was: $0 \text{ km}^3 \text{ s}^{-2} \leqslant GM_{\mathrm{PR}} \leqslant 4.22 \times 10^{-2} \text{ km}^3 \text{ s}^{-2}$ and $0 \leqslant GM_{\mathrm{PA}} \leqslant 2.52 \times 10^{-2} \text{ km}^3 \text{ s}^{-2}$, which is equivalent to densities ρ_{PR} and ρ_{PA} between 0 and 1.2 g cm⁻³, using the nominal volumes of Prometheus and Pandora given by Thomas (1989).

The first result is that all the solutions for which the rms error is typically $\lesssim 0.1″$ are such that $242° \leqslant \Delta\varpi_0 \leqslant 251°$. Our numerical fits thus provide a tighter constraint on the time of the latest apse anti-alignment, which occurred approximately between 2000 August 11 (epoch JED 2451767.5) and 2000 October 8 (epoch JED 2451825.5), using the apsidal precession rates of Prometheus and Pandora given by French et al. (2003).

The satellite masses we derived are given in Table 4. The rms error of this best-fit solution is $\mathrm{rms}_{\min} = 0.030″$, with comparable individual residuals for Prometheus and Pandora. This is equivalent to a mean error in the position of the satellites to about 190 km. Table 4 also contains for the best-fit solution the initial semi-major axes, resulting from Eqs. (3), and the initial periapse longitudes (corresponding to a difference $\Delta\varpi_0 = 250°$). Uncertainties in the satellite masses in Table 4 are the standard 3-σ errors. We have used constant χ^2 boundaries to define a 3-σ confidence level around the best-fit solution. This region is defined by $\mathrm{rms}^2 \leqslant \mathrm{rms}_{\min}^2(1 + \Delta\chi^2/N)$, where N is the number of data points, within which the rms increases by no more than a set amount $\Delta\chi^2$. For a 3-σ error, $\Delta\chi^2 = 14.2$ and $\mathrm{rms} \leqslant 0.033″$, this problem having three degrees of freedom M_{PR}, M_{PA}, and $\Delta\varpi_0$ (Press et al., 1986). Prometheus

Table 4
Prometheus and Pandora masses, together with the corresponding *GM* values and densities

	Prometheus	Pandora
M (10¹⁷ × kg)	$2.11^{+0.16}_{-0.37}\left[^{+0.79}_{-0.53}\right]$	$1.54^{+0.16}_{-0.28}\left[^{+0.50}_{-0.36}\right]$
GM (10⁻² × km³ s⁻²)	$1.41^{+0.10}_{-0.25}$	$1.03^{+0.10}_{-0.19}$
ρ (g cm⁻³)	$0.40^{+0.03}_{-0.07}\left[^{+0.15}_{-0.10}\right]$	$0.49^{+0.05}_{-0.09}\left[^{+0.16}_{-0.12}\right]$
a (km)	139377.43875	141714.28
ϖ (°)	249.0	359.0

The quoted uncertainties are the standard 3-σ errors. Small systematic effects due to the satellite eccentricities increase these 3-σ uncertainties to values given in the brackets (see text). The densities are derived using the nominal volumes given by Thomas (1989), and appear as black points in the map of rms residuals between the observations and the simulations (Fig. 3). Uncertainties in density arise only from those in M, because errors associated with the satellite volumes are not included. Also indicated are the initial semi-major axes and periapse longitudes for the best-fit solution (the eccentricities and the mean longitudes are the nominal values of Table 2).
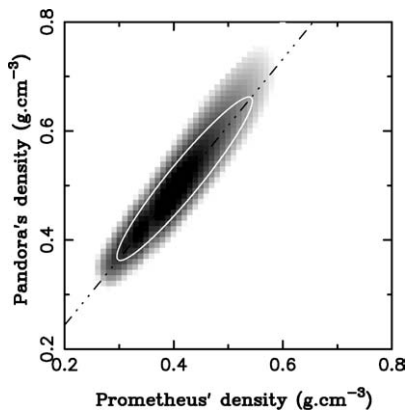
Fig. 3. Map of rms residuals between the observations and the numerical integrations, for given satellite densities (see text). The grey scale is such that white regions are for rms $\geqslant 0.05''$ and black regions are for rms $\leqslant 0.033''$, with a linear grey scale in between. The black area is almost an ellipse and corresponds to a 3-σ confidence level. The 3-σ errors extend to the white ellipse if we take into account small systematic effects due to the satellite eccentricities (see text). We have fitted the satellite masses (with eccentricities fixed at the nominal values of Table 2) and used the nominal volumes of Thomas (1989) to convert them into densities. Each point has its own initial orbital elements such that the rms error is minimal, given values of (ρ_{PR}, ρ_{PA}). Results are summarized in Table 4. The best fitting region is close to and parallel to the line $\rho_{PA}/\rho_{PR} = 1.22$, indicated by the dashed-dotted line, as a consequence of the conservation of angular momentum between the two satellites during the chaotic interactions (see text).

and Pandora densities given in Table 4 are computed using the nominal shape of the satellites (Thomas, 1989). Our results are compatible with the densities derived from the density waves excited in Saturn's rings by the two satellites: $\rho_{PR} = 0.27^{+0.16}_{-0.14}$, $\rho_{PA} = 0.42^{+0.28}_{-0.24}$ (Rosen et al., 1991). A map of the rms residuals for given satellite densities is also given in Fig. 3. The motion of each pair of masses was integrated several times, depending on the initial difference in longitude of periapsis, but we plot only the point for which the rms is minimal, using the nominal shape of the two moons (Thomas, 1989). There is a clear correlation in the masses (or the densities) we derive. Pandora's mass depends linearly on Prometheus' mass. This is a consequence of the conservation of angular momentum between Prometheus and Pandora during the chaotic interactions (see (15), (22), (23) of Goldreich and Rappaport, 2003b). The conservation of the angular momentum yields:

$$\frac{\Delta a_{PR}}{\Delta a_{PA}} = -\frac{M_{PA}}{M_{PR}} \frac{a^2_{PR}}{a^2_{PA}}. \qquad (4)$$

From French et al. (2003), $\Delta a_{PR} = +0.33$ km and $\Delta a_{PA} = -0.42$ km between 2000 and 2002, implying a mass ratio $M_{PR}/M_{PA} = 1.23$. The satellite masses we derived yield a comparable value $M_{PR}/M_{PA} = 1.37$, consistent with the previous value to within the uncertainties in the mass ratio. Using the nominal volumes of Thomas (1989), the density ratio is $\rho_{PA}/\rho_{PR} = 1.22$, indicated by the dashed-dotted line in Fig. 3. Note that using the satellite masses in Table 4 and the nominal volumes determined by Stooke (1993) or by Gozdziewski and Maciejewski (1995), Prometheus' density

is modified: $\rho_{PR} = 0.54^{+0.04}_{-0.09}$. The density of Pandora seems to be better constrained than that of Prometheus, because the volumes determined by Thomas (1989), Stooke (1993), and Gozdziewski and Maciejewski (1995) for this satellite are quite the same. Future images provided by the *Cassini* spacecraft will help to constrain the shapes of Saturn's satellites. The masses of Prometheus and Pandora will also be improved, because the next apse anti-alignment between the two satellites ($\sim$ 2006) will be seen by *Cassini*.

The longitude profiles of the best-fit solution (Table 4) are displayed in Fig. 1. Also indicated on the figure are two other solutions corresponding to satellite densities $\rho = 0$ and $1.2\ \mathrm{g\,cm^{-3}}$, respectively, for which the semi-major axes satisfy Eqs. (3) and the other initial orbital elements are the nominal values of Table 2. For illustration, we display the longitude offsets from the *Voyager* predictions, computed from the *HST* data sky-plane coordinates. They appear as small square points on the figure. However, these points are affected by the eccentricity of the two satellites, because we compute a true longitude, not a mean longitude, to derive the observed longitude lags. Indeed, we first compute the cartesian coordinates of the satellite in the saturnicentric reference frame ($O\mathbf{XYZ}$) described in Section 2. Because we consider equatorial orbits, we have:

$$\begin{cases} X = D\big[-(\Delta\alpha\cos\delta\cos P - \Delta\delta\sin P)\sin U \\ \qquad + (\Delta\alpha\cos\delta\sin P + \Delta\delta\cos P)\cos U/\sin B\big], \\ Y = D\big[(\Delta\alpha\cos\delta\cos P - \Delta\delta\sin P)\cos U \\ \qquad + (\Delta\alpha\cos\delta\sin P + \Delta\delta\cos P)\sin U/\sin B\big]. \end{cases} \qquad (5)$$

Then we convert X, Y into the radius r and the true longitude L of the satellite, we subtract from this longitude the mean longitude provided by the *Voyager* ephemeris (Evans, 2001) and we plot the mean value of the longitude offsets that correspond to the same *HST* visit, each set of observations typically including 5 closely-spaced measurements all taken at a single *HST* visit.

The rms error of the best-fit solution ($0.030''$) is slightly larger than the astrometric accuracy of the *HST* measurements ($\simeq 0.02''$). Therefore, either some systematic errors persist in the model, or the astrometric accuracy of the *HST* data is underestimated. Systematic errors could arise from various causes: inclinations of Prometheus and Pandora, different eccentricities from the assumed initial values, mass of the F ring, or highly sensitive effects of resonances with satellites, in particular Janus and Epimetheus, not properly taken into account in the initial conditions. However, we ran integrations applying small inclinations to Prometheus and Pandora, for various longitudes of ascending node, and this did not improve the rms residuals. On the other hand, we have fitted the eccentricities of Prometheus and Pandora to the non-chaotic region of data, with initial semi-major axes satisfying Eqs. (3) and for various initial longitudes of periapsis (consistent with the uncertainties given in Table 2). We obtained similar eccentricity values to the solutions of French et al. (2003). The residuals are not very sensitive to

Table 5
Predictions and uncertainties, during the *Cassini* tour, in the longitude off-sets from the *Voyager* ephemeris

Date (0h UT)	$\Delta\lambda_{PR}$ (°)	$\Delta\lambda_{PA}$ (°)
2004 July 1	$-29.74^{+0.16}_{-0.14}$	$31.97^{+0.16}_{-0.19}$
2008 July 1	$-36.27^{+2.36}_{-2.77}$	$38.79^{+3.92}_{-3.04}$

The $\Delta\lambda$'s are the difference between the mean longitude λ provided by the simulation and the mean longitude λ_{VGR} predicted by the ephemeris based on *Voyager* images (French et al., 2003; Evans, 2001). At the times considered, we compute the mean value of the longitude offsets and the uncertainties for the solutions given in Fig. 4.

this parameter, at least for values consistent with the uncertainties given in Table 2. Fits of the initial semi-major axes to the regular part of data with different initial eccentricity values yield also similar relations to Eqs. (3), with comparable residuals of about $0.03''$. Finally, we have also fitted the satellite masses and the initial longitudes of periapsis to the chaotic part of data using different initial eccentricity values. We have considered four extreme values of (e_{PR}, e_{PA}), consistent with the uncertainties given in Table 2: $(e_{PR}, e_{PA}) = (0.00171, 0.0042)$, $(0.00171, 0.0048)$, $(0.00213, 0.0042)$, and $(0.00213, 0.0048)$. The satellite masses are not significantly modified and the rms residuals are not improved. However, taking into account this small systematic effect enables us to estimate the increase of the uncertainties on the satellite masses we have determined. They are given into brackets in Table 4, and this corresponds to density values within the white ellipse in Fig. 3. Note that the forthcoming *Cassini* observations will help to constrain better the eccentricities of Prometheus and Pandora, and thus to reduce the uncertainties on the derived masses.

5. Orbital positions during the *Cassini* tour

Using our fit, we predict the orbital positions of the two satellites during the *Cassini* tour. We ran about 40 simulations with various initial conditions that fit the *HST* data quite well. The initial conditions used are in fact the best-fit solutions indicated by the black ellipse in Fig. 3, with rms errors $\leqslant 0.033''$. The results are displayed in Fig. 4. We also performed backward integrations, from the integration start time JED 2449940.0, to show that the longitude profiles are highly sensitive to initial conditions, and how the different solutions are distributed around the *Voyager* origin. The satellite masses cannot be constrained by the *Voyager* measurements. This results from the value of the Lyapunov time of about 3 yr. There are about 5 Lyapunov times between the integration start time and the *Voyager* origin. These simulations allow us to provide a lower limit of the uncertainties, due to chaos, in the positions of the satellites. Both for Prometheus and Pandora, these uncertainties amount to about $0.2°$ in mean longitude at the arrival of *Cassini* in July 2004, and to about $3°$ in 2008 (Table 5).
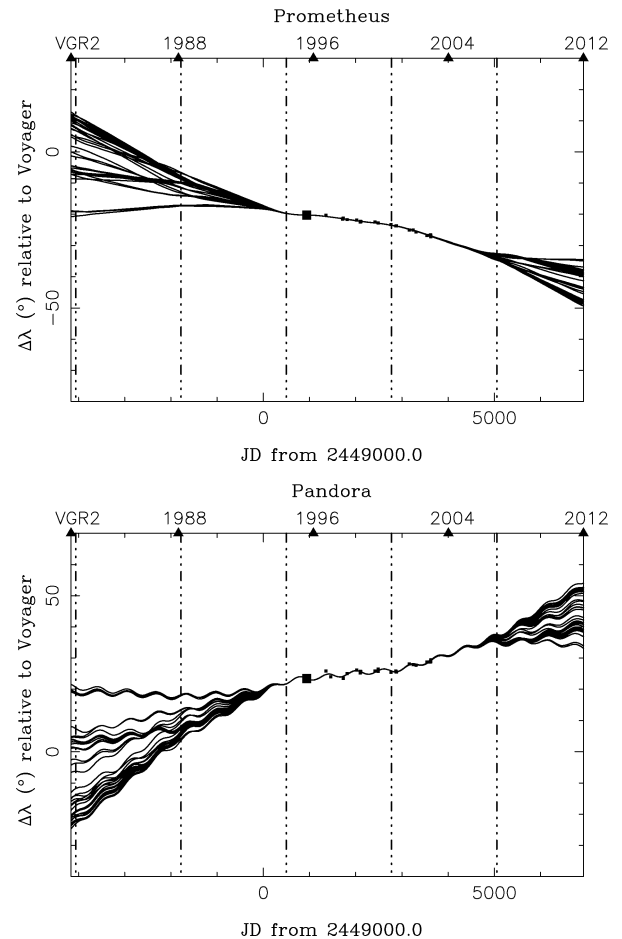
Fig. 4. Longitude offsets (degrees) from *Voyager* predictions for Prometheus (top) and Pandora (bottom) versus time (days). We ran about 40 simulations corresponding to the best-fit solutions (with rms $\leqslant 0.033''$) given in Fig. 3. The integration start time is 1995 August 10.5, indicated by the large square point. The vertical dashed-dotted lines denote the times of apse anti-alignment, computed using the apsidal precession rates of the two satellites given in French et al. (2003). The years 1988, 1996, 2004, 2012, and the *Voyager 2* origin (epoch JED 2444839.6682 $\simeq$ 1981 August 23) are labeled on the top horizontal axis. Backward integrations show how the solutions are distributed around the *Voyager* origin, as a consequence of chaos. Each small square point represents a separate set of *HST* data for which a single longitude offset $\Delta\lambda$ was computed from the observed sky-plane coordinates (see Fig. 1).

6. Conclusions

The recent *HST* observations enable us to constrain Prometheus and Pandora's densities, and also to give uncertainties on the positions of the satellites between 2004 and 2008. This is useful for future *Cassini* observations. Our results suggest that these moons are underdense. The residuals are slightly larger than the astrometric accuracy, suggesting that small systematic errors are still present in the model. Perhaps taking into account the effects of the F ring could improve the residuals, but this is difficult because we know little about the F ring mass. A more general study that includes fits to available *HST* observations of the co-orbitals Janus and Epimetheus should also be investigated.

Nevertheless, these low values for the densities raises the intriguing question of the origin of Prometheus and Pandora. Are Prometheus and Pandora the result of the accretion of ring material just outside the Roche zone of the planet? Did they form inside this region and migrate outward? Or do they result from the destruction of a former satellite that got close to the Roche zone? Given the satellite density values, the latter hypothesis seems to be less likely. Another interesting problem is the long-term dynamical evolution of the system. The new values for the masses and the improved orbits should allow a reexamination of the effect of the torques exerted on Prometheus and Pandora by Saturn's main rings, and help to constrain the lifetime of the system. *Cassini* observations during the upcoming four years will surely help to answer some of these questions.

Acknowledgments

Appendix A. Expressions for n and $\dot{\varpi}$

Here we give expressions for the apsidal precession rate and the mean motion up to and including terms in J_6. The orbital elements are *geometric* elements rather than classical osculating elements. These expressions are accurate to second order in eccentricity, and apply only for a test particle around an oblate planet (Borderies and Longaretti, 1987; Longaretti and Borderies, 1991; Borderies-Rappaport and Longaretti, 1994). Secular precession terms due to the major satellites are not included, because we are dealing with the short-term dynamical behavior of Prometheus and Pandora. These expressions are used to compute, iteratively, the geometric elements of Prometheus or Pandora from the state vectors in the numerical integrations.

$$n = \left(\frac{GM_S}{a^3}\right)^{1/2}\left[1 + \frac{3}{4}J_2\left(\frac{R_S}{a}\right)^2 - \frac{15}{16}J_4\left(\frac{R_S}{a}\right)^4\right.$$
$$+ \frac{35}{32}J_6\left(\frac{R_S}{a}\right)^6 - \frac{9}{32}J_2^2\left(\frac{R_S}{a}\right)^4 + \frac{45}{64}J_2J_4\left(\frac{R_S}{a}\right)^6$$
$$\left. + \frac{27}{128}J_2^3\left(\frac{R_S}{a}\right)^6 + 3J_2e^2\left(\frac{R_S}{a}\right)^2\right], \tag{A.1}$$

$$\dot{\varpi} = \left(\frac{GM_S}{a^3}\right)^{1/2}\left[\frac{3}{2}J_2\left(\frac{R_S}{a}\right)^2 - \frac{15}{4}J_4\left(\frac{R_S}{a}\right)^4\right.$$
$$+ \frac{105}{16}J_6\left(\frac{R_S}{a}\right)^6 - \frac{45}{32}J_2J_4\left(\frac{R_S}{a}\right)^6$$
$$\left. + \frac{27}{64}J_2^3\left(\frac{R_S}{a}\right)^6 + 3J_2e^2\left(\frac{R_S}{a}\right)^2\right]. \tag{A.2}$$

References

Bosh, A.S., Rivkin, A.S., 1996. Observations of Saturn's inner satellites during the May 1995 ring-plane crossing. Science 272, 518–521.

Borderies, N., Longaretti, P.-Y., 1987. Description and behavior of streamlines in planetary rings. Icarus 72, 593–603.

Borderies-Rappaport, N., Longaretti, P.-Y., 1994. Test particle motion around an oblate planet. Icarus 107, 129–141.

Campbell, J.K., Anderson, J.D., 1989. Gravity field of the saturnian system from Pioneer and Voyager tracking data. Astron. J. 97, 1485–1495.

Chambers, J.E., 1999. A hybrid symplectic integrator that permits close encounters between massive bodies. Mon. Not. R. Astron. Soc. 304, 793–799.

Cooper, N.J., Murray, C.D., 2004. Dynamical influences on the orbits of Prometheus and Pandora. Astron. J. 127, 1204–1217.

Dermott, S.F., 1981. The braided F-ring of Saturn. Nature 290, 454–457.

Dourneau, G., 1987. Observations et étude du mouvement des huit premiers satellites de Saturne. Thèse. Bordeaux, France.

Evans, M., 2001. The determination of orbits from spacecraft imaging. PhD thesis. Queen Mary College, University of London, UK.

Everhart, E., 1985. An efficient integrator that uses Gauss–Radau spacings. In: Carusi, A., Valsecchi, G.B. (Eds.), Dynamics of Comets: Their Origin and Evolution. Reidel, Dordrecht, pp. 185–202.

French, R.G., McGhee, C.A., 2003. HST astrometry of Saturn's small satellites. Bull. Am. Astron. Soc. 34, 06.07. DDA meeting abstract.

French, R.G., 17 colleagues, 1993. Geometry of the Saturn system from the 3 July 1989 occultation of 28 Sgr and Voyager observations. Icarus 103, 163–214.

French, R.G., McGhee, C.A., Dones, L., Lissauer, J.J., 2003. Saturn's wayward shepherds: the peregrinations of Prometheus and Pandora. Icarus 162, 143–170.

Giuliatti Winter, S.M., Murray, C.D., Gordon, M., 2000. Perturbations to Saturn's F-ring strands at their closest approach to Prometheus. Planet. Space Sci. 48, 817–827.

Goldreich, P., Rappaport, N., 2003a. Chaotic motions of Prometheus and Pandora. Icarus 162, 391–399.

Goldreich, P., Rappaport, N., 2003b. Origin of chaos in the Prometheus–Pandora system. Icarus 166, 320–327.

Goldreich, P., Tremaine, S., 1979. Towards a theory for the uranian rings. Nature 277, 97–99.

Gozdziewski, K., Maciejewski, A.J., 1995. On the gravitational fields of Pandora and Prometheus. Earth Moon Planets 69, 25–50.

Harper, D., Taylor, D.B., 1993. The orbits of the major satellites of Saturn. Astron. Astrophys. 268, 326–349.

Kolvoord, R.A., Burns, J.A., Showalter, M.R., 1990. Periodic features in Saturn's F ring: evidence for nearby moonlets. Nature 345, 695–697.

Lissauer, J.J., Peale, S.J., 1986. The production of 'braids' in Saturn's F ring. Icarus 67, 358–374.

Longaretti, P.Y., Borderies, N., 1991. Streamline formalism and ring orbit determination. Icarus 94, 165–170.

McGhee, C.A., 2000. Comet Shoemaker–Levy's 1994 with Jupiter and Saturn's 1995 ring plane crossing. PhD thesis. Cornell University, Ithaca, NY.

McGhee, C.A., Nicholson, P.D., French, R.G., Hall, K.J., 2001. HST observations of saturnian satellites during the 1995 ring plane crossings. Icarus 152, 282–315.

Murray, C.D., Giuliatti Winter, S.M., 1996. Periodic collisions between the moon Prometheus and Saturn's F ring. Nature 380, 139–141.

Murray, C.D., Gordon, M.K., Giuliatti Winter, S.M., 1997. Unraveling the strands of Saturn's F ring. Icarus 129, 304–316.

Murray, C.D., Evans, M.W., Porco, C.C., Showalter, M.R., 2000. The orbits of Prometheus, Pandora and Atlas in 1980 and 1981. Bull. Am. Astron. Soc. 32, 1090. DPS meeting abstract.

Namouni, F., 1998. Ringlet–satellite interactions. Mon. Not. R. Astron. Soc. 300, 915–930.

Nicholson, P.D., Porco, C.C., 1988. A new constraint on Saturn's zonal gravity harmonics from Voyager observations of an eccentric ringlet. J. Geophys. Res. 93, 10209–10224.

Nicholson, P.D., Hamilton, D.P., Matthews, K., Yoder, C.F., 1992. New observations of Saturn's coorbital satellites. Icarus 100, 464–484.

Nicholson, P.D., Showalter, M.R., Dones, L., French, R.G., Larson, S.M., Lissauer, J.J., McGhee, C.A., Sicardy, B., Seitzer, P., Danielson, G.E., 1996. Observations of Saturn's ring-plane crossings in August and November 1995. Science 272, 509–515.

Poulet, F., Sicardy, B., 2001. Dynamical evolution of the Prometheus–Pandora system. Mon. Not. R. Astron. Soc. 322, 343–355.

Press, W.H., Teukolsky, S.A., Vetterling, W.T., Flannery, B.P., 1986. Numerical Recipes. Cambridge Univ. Press, Cambridge, UK.

Renner, S., Sicardy, B., 2003. Consequences of the chaotic motions of Prometheus and Pandora. Bull. Am. Astron. Soc. 35, 04.06. DPS meeting abstract.

Rosen, P.A., Tyler, G.L., Marouf, E.A., Lissauer, J.J., 1991. Resonance structure in Saturn's rings probed by radio occultation. II. Icarus 93, 25–44.

Showalter, M.R., 2004. Disentangling Saturn's F ring. I. Clump orbits and lifetimes. Icarus 171, 356–371.

Showalter, M.R., Burns, J.A., 1982. A numerical study of Saturn's F ring. Icarus 52, 526–544.

Showalter, M.R., Dones, L., Lissauer, J.J., 1999a. Revenge of the sheep: effects of Saturn's F ring on the orbit of Prometheus. Bull. Am. Astron. Soc. 31, 1441. DPS meeting abstract.

Showalter, M.R., Dones, L., Lissauer, J.J., 1999b. Interactions between Prometheus and the F ring. Bull. Am. Astron. Soc. 31, 1228. DPS meeting abstract.

Stooke, P.J., 1993. The shapes and surfaces of Prometheus and Pandora. Earth Moon Planets 62, 199–221.

Synnott, S.P., Peters, C.F., Smith, B.A., Morabito, L.A., 1981. Orbits of the small satellites of Saturn. Science 212, 191–192.

Synnott, S.P., Terrile, R.J., Jacobson, R.A., Smith, B.A., 1983. Orbits of Saturn's F ring and its shepherding satellites. Icarus 53, 156–158.

Thomas, P.C., 1989. The shapes of small satellites. Icarus 77, 248–274.

Vienne, A., Duriez, L., 1995. TASS1.6: Ephemerides of the major saturnian satellites. Astron. Astrophys. 297, 588–605.

Yoder, C.F., Synnott, S.P., Salo, H., 1989. Orbits and masses of Saturn's co-orbiting satellites, Janus and Epimetheus. Astron. J. 98, 1875–1889.